EPJ manuscript
—

Vector Correlators in Lattice QCD: methods and applications

David Bernecker[1] and Harvey B. Meyer[1]

Institut für Kernphysik, Johannes Gutenberg Universität Mainz, 55099 Mainz, Germany

July 25, 2011

Abstract. We discuss the calculation of the leading hadronic vacuum polarization in lattice QCD. Exploiting the excellent quality of the compiled experimental data for the $e^+e^- \to$ hadrons cross-section, we predict the outcome of large-volume lattice calculations at the physical pion mass, and design computational strategies for the lattice to have an impact on important phenomenological quantities such as the leading hadronic contribution to $(g-2)_\mu$ and the running of the electromagnetic coupling constant. First, the $R(s)$ ratio can be calculated directly on the lattice in the threshold region, and we provide the formulae to do so with twisted boundary conditions. Second, the current correlator projected onto zero spatial momentum, in a Euclidean time interval where it can be calculated accurately, provides a potentially critical test of the experimental $R(s)$ ratio in the region that is most relevant for $(g-2)_\mu$. This observation can also be turned around: the vector correlator at intermediate distances can be used to determine the lattice spacing in fm, and we make a concrete proposal in this direction. Finally, we quantify the finite-size effects on the current correlator coming from low-energy two-pion states and provide a general parametrization of the vacuum polarization on the torus.

PACS. 12.38.Gc – 13.40.Gp – 13.66.Bc

1 Introduction

In quantum field theory, the information encoded in the correlation functions of conserved currents has important phenomenological applications. The correlation function of the electromagnetic current, in particular, quantifies the polarization of the 'vacuum' by virtual particles induced by the passage of a photon. This virtuality-dependent vacuum polarization $\Pi(Q^2)$ affects the propagation of the photon and has physically observable consequences, see for instance [1]. One of them is the running of the fine structure constant $\alpha(Q^2)$, which now depends on the four-momentum squared of the photon via Eq. (11) below. Another consequence of the polarization of the vacuum is a contribution of all virtual particles to the magnetic moments of leptons, which can be measured to very high precision in the case of the electron and the muon (see [2] for a review of the subject). We will discuss this application extensively below.

One important contribution to the vacuum polarization comes from QCD. At high virtuality Q^2, this contribution to $\Pi(Q^2)$ is calculable in perturbation theory, due to the asymptotic freedom property of QCD. Below a scale of a few GeV, the vacuum polarization receives large non-perturbative contributions, making it inaccessible to known analytic methods. From here on, we will focus exclusively on the QCD contribution to $\Pi(Q^2)$, but will keep using the same symbol. In particle phenomenology, it has been customary to extract the low-Q^2 part of the function $\Pi(Q^2)$ from experiments via a dispersion relation (Eq. 16 below). However it is also possible to directly calculate $\Pi(Q^2)$ from first principles using numerical lattice QCD methods [3,4,5,6], roughly for a range of momenta $0.1\text{GeV}^2 \lesssim Q^2 \lesssim 4.0\text{GeV}^2$. What limits the upper end of the momentum range is the size of the lattice spacing a, whose inverse provides a momentum cutoff $\sim \pi/a$. On the lower end, it is the discreteness of the available momenta in a finite volume ($|Q_{\min}| = \frac{2\pi}{L}$ on a torus of dimension L) that limits the accessible Q^2 values. We note that current correlators involving heavy flavors of quarks have been used on the lattice for other purposes, namely determining the charm quark mass and the QCD coupling constant [7].

To obtain the leading hadronic contribution to the anomalous magnetic moment of the muon a_μ^{HLO}, the imaginary part of the vacuum polarization at timelike momenta is folded with an analytically known QED kernel [8] which involves only the scale m_μ. An important observation of Blum [3] was that the same quantity a_μ^{HLO} can also be expressed as an integral over spacelike momenta. This opens the possibility to evaluate it in the Euclideanized theory, which can be simulated non-perturbatively by Monte-Carlo methods [3,4,5,6]. Because the muon mass $\mu \approx 105\text{MeV}$ is small on hadronic scales, the contribution to a_μ is dominated by the region of small Q^2 or, alternatively, by long distance contributions. How exactly this affects the calculation is one topic we will address.

Since the vector spectral function is already extremely well known from particle physics experiments, only highly accurate lattice predictions will have a useful impact on phenomenology. By the same token, the knowledge of the vector spectral function allows us to design useful observables which are both accurately computable on the lattice and critically challenge the experimental measurements that are relevant to the determination of $\Delta\alpha(M_Z^2)$ and $a_\mu^{\rm HLO}$.

One of our goals will be to understand some of the systematic errors that may affect the direct lattice calculation of the vacuum polarization. A second goal is to propose other promising computational strategies, in increasing level of 'ambition', which we believe could have a phenomenological impact. These strategies represent a compromise between computational feasability and phenomenological relevance. The third topic is our proposal of a new reference scale τ_0 which is both accurately calculable on the lattice and extractable from experimental data with negligible model dependence. The time-scale τ_0 is defined from the isospin vector current correlator.

In section (2), after a review of the basic relations between the relevant observables, we provide a comparison of the vacuum polarization calculated on the lattice and the vacuum polarization obtained from the phenomenological R ratio by employing the dispersion relation (10). We observe that even state-of-the-art lattice calculations still yield a vacuum polarization about a factor of two smaller than phenomenology indicates in a wide range of momenta. In section (3), we provide the general parametrization of the polarization tensor $\Pi_{\mu\nu}(Q)$ compatible with the symmetries of the torus and the conservation of the electromagnetic current; this allows one to perform several tests of finite-volume effects. In section (4) we will switch to the mixed representation $(t, \boldsymbol{q})$, where t is Euclidean time, which facilitates the interpretation of the vector correlator in terms of physical states. At large times t, the current correlator is exponentially dominated by the low-lying states. These are two-pion states on the torus and due to the sparsity of momenta available to them, their contribution is affected by O(1) finite volume effects. Based on this understanding, we will consider three ways in which the lattice could have an impact on the determination of $\Delta\alpha(Q^2 = M_Z^2)$ and $a_\mu^{\rm HLO}$. Section (5) describes the new reference scale τ_0. In section (6), we present a technical generalization of the Lüscher formula in the vector channel for twisted boundary conditions (see also [9] in the scalar channel), which are expected to help in the determination of the timelike pion form factor. The concluding section contains a summary of our findings and proposed computational strategies.

2 Preliminaries and status of vacuum polarization determinations

We begin this section by introducing the relevant quantities and reviewing the most important relations among them. This will allow us to perform a comparison between lattice experimental data. Our Minkowski metric convention is $(+---)$. Euclidean momenta are denoted by a capital letter, Minkowski momenta by a small letter.

The electromagnetic current

$$j_\mu^{\rm em} = \tfrac{2}{3}\bar{u}\gamma_\mu u - \tfrac{1}{3}\bar{d}\gamma_\mu d - \tfrac{1}{3}\bar{s}\gamma_\mu s + \dots \tag{1}$$

is the central operator of interest in this paper. The corresponding spectral function is defined as

$$\rho_{\mu\nu}(k) \equiv \frac{1}{2\pi}\int d^4x\, e^{ik\cdot x}\langle 0|[j_\mu^{\rm em}(x), j_\nu^{\rm em}(0)]|0\rangle. \tag{2}$$

Due to current conservation and Lorentz invariance, the tensor structure of $\rho_{\mu\nu}$ is

$$\rho_{\mu\nu}(k) = (k_\mu k_\nu - g_{\mu\nu}k^2)\cdot\rho(k^2). \tag{3}$$

The spectral density ρ is non-negative. In the free theory for massless quarks of charges Q_f, it is given by a step function,

$$\rho(s) = \frac{N_c(\sum_f Q_f^2)}{12\pi^2}\,\theta(s) \qquad \text{(free massless quarks)}. \tag{4}$$

More generally, $\rho(s)$ is related to experimental observables by the optical theorem,

$$\rho(s) = \frac{R(s)}{12\pi^2}, \qquad R(s) \equiv \frac{\sigma(e^+e^-\to\text{hadrons})}{4\pi\alpha(s)^2/(3s)}. \tag{5}$$

The denominator is the treelevel cross-section $e^+e^-\to\mu^+\mu^-$ in the limit $s\gg m_\mu^2$, and we have neglected QED corrections. At low energies, the spectral density is given by the pion form factor [2],

$$\rho(s) = \frac{1}{48\pi^2}\Big(1-\frac{4m_\pi^2}{s}\Big)^{\frac{3}{2}}|F_\pi(\sqrt{s})|^2, \qquad |F_\pi(0)| = 1. \tag{6}$$

This relation holds near threshold, $2m_\pi \le \sqrt{s} \le 3m_\pi$, and even up to $4m_\pi$ if the electromagnetic current is replaced by the isospin current in the definition of $\rho(s)$. In [10], a formula relating the pion form factor to a finite-volume matrix element calculable in lattice QCD was derived,

$$|F_\pi(E)|^2 = \Big(q\phi'(q) + k\frac{\partial\delta_1(k)}{\partial k}\Big)\frac{3\pi E^2}{k^5}|A_\psi|^2. \tag{7}$$

Here E equals the invariant mass of the two pions, k is related to E via $E = 2\sqrt{m_\pi^2+k^2}$, δ_1 is the scattering phase shift in the p-wave, isospin $I=1$ channel and A_ψ is a vector-current matrix element between the vacuum and a unit-norm two-pion state $|\psi_\sigma^a\rangle$ of energy E on the torus. Finally, $q \equiv \frac{kL}{2\pi}$ and ϕ is a known kinematic function [11]. The scattering phase $\delta_1(k)$ can be extracted (see [12,13] and Refs. therein) from the finite-volume spectrum using the Lüscher formula [14,11].

In Euclidean space, the natural object is the polarization tensor

$$\Pi_{\mu\nu}(Q) \equiv \int d^4x\, e^{iQ\cdot x}\langle j_\mu(x)j_\nu(0)\rangle, \tag{8}$$

and O(4) invariance and current conservation imply the tensor structure

$$\Pi_{\mu\nu}(Q) = \big(Q_\mu Q_\nu - \delta_{\mu\nu}Q^2\big)\Pi(Q^2). \tag{9}$$

The function $\Pi(Q^2)$ can be calculated in lattice QCD [3, 4, 5, 6]. The leading hadronic contribution to the vacuum polarization $e^2\Pi(Q^2)$ in the spacelike domain can be expressed through the spectral function via a once-subtracted dispersion relation,

$$\Pi(Q^2) - \Pi(0) = Q^2 \int_0^\infty \mathrm{d}s \frac{\rho(s)}{s(s+Q^2)}. \tag{10}$$

An important physical application of the vacuum polarization is the running of the electromagnetic coupling,

$$\alpha(Q^2) = \frac{\alpha}{1 - \Delta\alpha(Q^2)}, \qquad \alpha \equiv \alpha(0), \tag{11}$$
$$\Delta\alpha(Q^2) = 4\pi\alpha\,\mathrm{Re}\,\big[\Pi(Q^2) - \Pi(0)\big].$$

In particular the value of the coupling at the scale $Q^2 = M_Z^2$ is a precision observable that, combined with the Fermi constant, the Z boson mass, the quark masses and the Higgs mass, lead to a prediction for the Weinberg angle, which confronted with its direct measurement leads to an upper bound on the Standard Model Higgs boson mass (see for instance [1]).

The $\mathrm{O}(\alpha^2)$ hadronic contribution to the muon anomalous magnetic moment can be expressed in terms of $\Pi(Q^2)$ as

$$a_\mu^{\mathrm{HLO}} = \Big(\frac{\alpha}{\pi}\Big)^2 \int_0^\infty \mathrm{d}Q^2 K_E(Q^2)\widehat{\Pi}(Q^2), \tag{12}$$
$$\widehat{\Pi}(Q^2) = 4\pi^2\big[\Pi(Q^2) - \Pi(0)\big], \tag{13}$$

with the kernel given by[1] [3]

$$K_E(s) = \frac{1}{m_\mu^2}\cdot\hat{s}\cdot Z(\hat{s})^3\cdot\frac{1-\hat{s}Z(\hat{s})}{1+\hat{s}Z(\hat{s})^2}, \tag{14}$$
$$Z(\hat{s}) = -\frac{\hat{s}-\sqrt{\hat{s}^2+4\hat{s}}}{2\hat{s}}, \quad \hat{s} = \frac{s}{m_\mu^2}. \tag{15}$$

Eq. (12) is used to obtain a_μ^{HLO} based on the vacuum polarization computed on the lattice.

2.1 Confronting the vacuum polarization from the lattice and the $R(s)$ ratio via the dispersion relation

The vacuum polarization can be easily calculated from the $R(s)$ ratio by using the optical theorem (5) and the dispersion relation (10). In the Euclidean domain, the relation reads

$$\widehat{\Pi}(Q^2) = \frac{Q^2}{3}\int_0^\infty ds \frac{R(s)}{s(s+Q^2)}. \tag{16}$$

[1] Our function K_E matches the function f introduced in [3].

	C_i	M_i/GeV	Γ_i/GeV
0	655.5	0.7819	0.0358
1	8.5	0.7650	0.130
2	11.5	0.7820	0.00829
3	50.0	1.0195	0.00426

Table 1: Parameters used in the parametrization (18) of the $R(s)$ ratio.

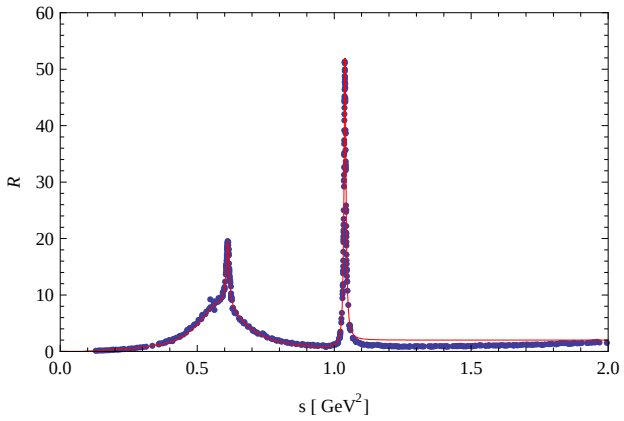

Fig. 1: Parametrization of the $R(s)$ ratio.

By taking the phenomenological determination of $R(s)$, the integral can be evaluated and a comparison to the vacuum polarization calculated on the lattice is possible. For this purpose we parametrize the $R(s)$ ratio using Breit-Wigner curves of the form

$$f(\sqrt{s}) = \frac{C\,\Gamma^2}{4(\sqrt{s}-M)^2+\Gamma^2} \tag{17}$$

where the parameters C, M, Γ are used to match the height of the resonance to the experimental data compiled by the Particle Data Group (PDG) [15]. Altogether our parametrization reads, for s in units of GeV^2,

$$\begin{aligned} R(s) = {} & \theta(\sqrt{s}-2m_{\pi^\pm})\,\theta(4.4m_{\pi^\pm}-\sqrt{s}) \\ & \tfrac{1}{4}\Big[1-\tfrac{4m_{\pi^\pm}^2}{s}\Big]^{3/2}\big(0.6473+f_0(\sqrt{s})\big) \\ & +\theta(\sqrt{s}-4.4m_{\pi^\pm})\theta(M_3-\sqrt{s})\Big(\textstyle\sum_{i=1}^2 f_i(\sqrt{s})\Big) \\ & +f_3(\sqrt{s}) + 3\big((\tfrac{2}{3})^2+(\tfrac{1}{3})^2+(\tfrac{1}{3})^2\big)\theta(\sqrt{s}-M_3). \end{aligned} \tag{18}$$

To the f_i correspond the parameters $\{C_i, M_i, \Gamma_i\}$ listed in Tab. (1).

A comparison between the parametrization and the experimental data compiled by the PDG can be seen in figure 1. The vacuum polarization resulting from integrating our parametrization of $R(s)$ in Eq. (16) is shown in figure (2). With the calculated vacuum polarization it is also possible to calculate the hadronic contribution to the anomalous magnetic moment of the muon a_μ^{HLO} by using formula (12). Using our simple parametrization of the $R(s)$ ratio, we obtaine the value $a_\mu^{\mathrm{HLO}} = 672\cdot10^{-10}$. It is close enough to the reference value of $a_\mu^{\mathrm{HLO}} = (690.3\pm5.3)\cdot10^{-10}$ [17]

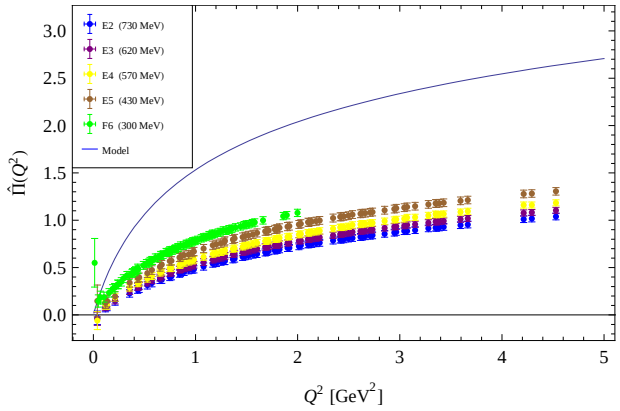

Fig. 2: Comparison of the vacuum polarization calculated using our parametrization (18) of the $R(s)$ ratio and lattice data from [16,6].

(see the review [2] and the recent [18,19] for the latest evaluations) for the purpose of this article to justify the simple functional form we have used.

The phenomenological hadronic vacuum polarization is compared to lattice QCD data generated by Della Morte et al. [16,6][2] in Fig. (2). The data is generated from $N_{\rm f} = 2$ gauge field configurations, i.e. they only include the sea quark effects of the u, d quarks. In the electromagnetic current, the contributions of the up, down and strange quarks were taken into account. Results at different light-quark masses are displayed in Fig. (2), corresponding to 'pion' masses m_π down to 300MeV. The E lattices are $32^3 \times 64$ and the F lattices are $48^3 \times 96$, so that the smallest value of $m_\pi L$ is 4.7. Only the Wick-connected contributions were included in the calculation. Twisted boundary conditions were used to obtain the vacuum polarization at a denser set of momenta. For more details, we refer the reader to the original publications [16,6].

The subtracted vacuum polarization $\widehat{\Pi}(Q^2)$ calculated on the lattice lies about a factor two below the curve obtained using the experimental $R(s)$ ratio. As the quark mass is lowered, the curves (very slowly) approach the phenomenological curve. So in spite of the excellent statistical quality of the lattice data, the large volumes used, and the dense set of momenta, a large difference remains between the lattice and the phenomenological curve. And this occurs in a region (say, $0.4\text{GeV}^2 < Q^2 < 2.0\text{GeV}^2$) where we would expect cutoff effects to be small. We note however that in view of the form of kernel $K(s)$, this region makes only a modest contribution to $a_\mu^{\rm HLO}$, and that the smallness of $a_\mu^{\rm HLO}$ calculated around $m_\pi = 300$MeV is instead related to the behavior of $\Pi(Q^2)$ very close to the origin (barely visible in Fig. 2). In fact, in the limit where the lepton mass goes to zero, the hadronic contribution to its anomalous magnetic moment is given by

$$\lim_{m_\mu \to 0} \frac{a_\mu^{\rm HLO}}{m_\mu^2} = \frac{1}{3}\left(\frac{\alpha}{\pi}\right)^2 \left(\frac{\widehat{\Pi}(s)}{s}\right)_{s=0}. \qquad (19)$$

Feng et al. [5] followed an approach based on the idea that using the variable Q^2/m_ρ^2 for the horizontal axis, where m_ρ is the quark-mass dependent ρ-meson mass, leads to an approximate scaling at small Q^2, in the sense that the curves corresponding to different quark masses would approximately lie on top of eachother. This idea may prove helpful in carrying out the chiral extrapolation, but it only partly explains the difference between the curves in Fig. (2).

The different channels contributing to $R(s)$ and their relative importance for the evaluation of the vacuum polarization and $a_\mu^{\rm HLO}$ have been described in the literature, Refs. [20,18,19,2] among others. For the reader's convenience we summarize some of the facts known from e^+e^- annihilation experiments that are relevant to our discussion. The total two-pion contribution represents roughly 75% of $a_\mu^{\rm HLO}$, and it is itself dominated by the $\rho(770)$ meson contribution: the part of it that comes from below 0.5GeV amounts to 8.4% [21], while the two-pion contribution to $a_\mu^{\rm HLO}$ from $0.1 \le s \le 0.85\text{GeV}^2$ is 69% [22, 23]. See in particular the accurate initial-state radiation (ISR) measurements in this region [24,23]; the world's data is nicely summarized in Fig. (3) of Ref. [19]. The point has also been made [25] that if the energy region below 500MeV was alone responsible for the current discrepancy between the Standard Model prediction and the direct measurement of $a_\mu^{\rm HLO}$, it would require a 52% increase of the $e^+e^- \to \pi^+\pi^-$ cross section, and it would then also lead to a lowered Higgs mass upper-bound of 143GeV at 95% confidence level. Such an increase seems very unlikely in view of the quoted experimental errors.

For comparison, the entire three-pion contribution to $a_\mu^{\rm HLO}$ from threshold to 1.8GeV is about 6.8% [19,18] (see Fig. (13) of [19]). From threshold to 660MeV, Hagiwara et al. [19] estimate it in Chiral Perturbation Theory to be negligible, 0.001%. The four-pion contribution has also been determined. From 0.305 to 1.8GeV, the $2\pi^+2\pi^-$ channel yields 2.0%, while $\pi^+\pi^-2\pi^0$ yields 2.7% [19].

We note that a lattice calculation containing just the Wick-connected diagrams of the up and down quarks amounts to working with the isospin current. Such a calculation can perfectly well be compared to the experimental data if one selects unit isospin final hadronic states. In particular, the ω and ϕ resonances should not be included in the dispersion integral in such a comparison. See also [26] for an analysis of the Wick-disconnected diagrams in chiral perturbation theory.

3 The vacuum polarization on the torus

As in all numerical lattice QCD calculations, the vacuum polarization is evaluated in finite volume. We will assume that the boundary conditions are periodic in all directions,

[2] A more extensive set of these lattice results was reviewed by J. Zanotti in a plenary session of the Hadron 2011 conference, Munich, 13-17 June 2011.

except that the fermions have antiperiodic boundary conditions in the time direction (the system is thus at a finite, albeit low temperature). The question then arises, how large the finite-size effects are, and what their parametric dependence is. A first step towards answering this question is to provide a general parametrization of the polarization tensor on the torus of dimensions $\beta \times L^3$.

The correlation function of a (not necessarily conserved) current forms a rank-two symmetric tensor which can be uniquely decomposed into a traceless and a scalar component,

$$\Pi_{\mu\nu}(q) = \bar{\Pi}_{\mu\nu}(q) + \hat{\Pi}_{\mu\nu}(q), \tag{20}$$
$$\hat{\Pi}_{\mu\nu}(q) = \delta_{\mu\nu}\hat{\Pi}(q), \qquad \sum_{\mu=0}^{3}\bar{\Pi}_{\mu\mu}(q) = 0. \tag{21}$$

In infinite space ($\mathbb{R}^4$), the O(4) symmetry of the theory implies that

$$\bar{\Pi}_{\mu\nu}(q) = (q_\mu q_\nu - \frac{1}{d}\delta_{\mu\nu}q^2)f(q^2), \tag{22}$$
$$\hat{\Pi}_{\mu\nu}(q) = \delta_{\mu\nu}q^2 g(q^2). \tag{23}$$

Imposing the conservation equation $q_\mu \Pi_{\mu\nu}(q) = 0$, we obtain the condition

$$g(q^2) = -\frac{d-1}{d}f(q^2). \tag{24}$$

Returning to Eq. (20), one then arrives at (9),

$$\Pi_{\mu\nu}(q) = (q_\mu q_\nu - \delta_{\mu\nu}q^2)f(q^2), \tag{25}$$

and $f(q^2)$ can be identified with the vacuum polarization, usually notated $\Pi(q^2)$.

On a four-dimensional torus of dimensions L^4, the relevant symmetry group is the hypercubic group H(4). We will follow the notation of Ref. [27]. The 20 inequivalent irreducible representations of H(4) are denoted by $\tau_k^{(l)}$, where l is the dimension of the representation and $k = 1, 2, \ldots$ distinguishes inequivalent representations of the same dimension. There are four one-dimensional representations, two of dimension two; four of dimension three, four, and six; and two of dimension eight. The defining representation is labeled as $\tau_1^{(4)}$. The currents $j_\mu(x)$ belong to this representation. Their direct product can be decomposed according to [27]

$$\tau_1^{(4)} \otimes \tau_1^{(4)} = \tau_1^{(1)} \oplus \tau_1^{(3)} \oplus \tau_1^{(6)} \oplus \tau_3^{(6)}. \tag{26}$$

Because the vector correlator is symmetric in the space-time indices μ and ν, the antisymmetric representation $\tau_1^{(6)}$ will play no role in the following.

Very often the space on which QCD is simulated is a four-dimensional torus of dimensions $\beta \times L^3$. Then the symmetry group H(4) is further reduced to $Z(2) \times$ H(3), where $Z(2)$ corresponds to Euclidean-time reversal and H(3) is the symmetry group of the cube. Two irreducible representations of H(4) appearing in Eq. (26) further break up into smaller irreducible representations of H(3). The latter are denoted A_1, A_2, E, T_1 and T_2 (respectively of dimensions 1, 1, 2, 3 and 3). We then have the decompositions

$$\tau_3^{(6)} = T_1 \oplus T_2, \tag{27}$$
$$\tau_1^{(3)} = A_1 \oplus E. \tag{28}$$

Thus

$$\bar{\Pi}_{\mu\nu}(q) = \bar{\Pi}_{\mu\nu}^{A_1}(q) + \bar{\Pi}_{\mu\nu}^{E}(q) + \bar{\Pi}_{\mu\nu}^{T_1}(q) + \bar{\Pi}_{\mu\nu}^{T_2}(q), \tag{29}$$
$$\hat{\Pi}_{\mu\nu}(q) = \delta_{\mu\nu}\hat{\Pi}^{A_1}(q). \tag{30}$$

In matrix notation, we now have (all matrices are symmetric)

$$\bar{\Pi}_{\mu\nu}^{A_1}(q) = \begin{pmatrix} \bar{\Pi}_{00}^{A_1} & 0 & 0 & 0 \\ & \frac{-1}{3}\bar{\Pi}_{00}^{A_1} & 0 & 0 \\ & & \frac{-1}{3}\bar{\Pi}_{00}^{A_1} & 0 \\ & & & \frac{-1}{3}\bar{\Pi}_{00}^{A_1} \end{pmatrix}, \tag{31}$$

$$\bar{\Pi}_{\mu\nu}^{E}(q) = \begin{pmatrix} 0 & 0 & 0 & 0 \\ & \bar{\Pi}_{11}^{E} & 0 & 0 \\ & & \bar{\Pi}_{22}^{E} & 0 \\ & & & \bar{\Pi}_{33}^{E} \end{pmatrix}, \ \sum_{j=1}^{3}\bar{\Pi}_{jj}^{E} = 0, \tag{32}$$

$$\bar{\Pi}_{\mu\nu}^{T_1}(q) = \begin{pmatrix} 0 & \bar{\Pi}_{01}^{T_1} & \bar{\Pi}_{02}^{T_1} & \bar{\Pi}_{03}^{T_1} \\ & 0 & 0 & 0 \\ & & 0 & 0 \\ & & & 0 \end{pmatrix}, \tag{33}$$

$$\bar{\Pi}_{\mu\nu}^{T_2}(q) = \begin{pmatrix} 0 & 0 & 0 & 0 \\ & 0 & \bar{\Pi}_{12}^{T_2} & \bar{\Pi}_{13}^{T_2} \\ & & 0 & \bar{\Pi}_{23}^{T_2} \\ & & & 0 \end{pmatrix}. \tag{34}$$

Without using the conservation of the current, $\Pi_{\mu\nu}(q)$ is thus characterized by five independent functions belonging to various irreducible representations of the group H(3).

The Ward identities still read $q_\mu \Pi_{\mu\nu}(q) = 0$ on the torus. Writing them out for $\nu = 0$ and 1,

$$q_0\big(\bar{\Pi}_{00}^{A_1} + \hat{\Pi}^{A_1}\big) = -\textstyle\sum_{j=1}^{3} q_j \bar{\Pi}_{0j}^{T_1} \tag{35}$$
$$q_1\big(\hat{\Pi}^{A_1} + \bar{\Pi}_{11}^{E} - \tfrac{1}{3}\bar{\Pi}_{00}^{A_1}\big) = -q_0\bar{\Pi}_{01}^{T_1} - q_2\bar{\Pi}_{12}^{T_2} - q_3\bar{\Pi}_{13}^{T_2}. \tag{36}$$

There are two further equations obtained from Eq. (36) by cyclic permutation of the indices (1,2,3). The three representations parametrizing the diagonal components can be related to the two off-diagonal representations T_1 and T_2. For a generic momentum with non-vanishing components in each direction, we have the relations

$$4\bar{\Pi}^{A_1}(q) = \sum_{i\neq j}\bar{\Pi}_{ij}^{T_2}\frac{q_i}{q_j} - \sum_j \bar{\Pi}_{0j}^{T_1}\big(3\frac{q_j}{q_0} + \frac{q_0}{q_j}\big), \tag{37}$$
$$4\hat{\Pi}^{A_1}(q) = -\sum_{i\neq j}\bar{\Pi}_{ij}^{T_2}\frac{q_i}{q_j} - \sum_j \Pi_{0j}\big(\frac{q_j}{q_0} + \frac{q_0}{q_j}\big). \tag{38}$$

If one or more components of the momentum vanish, one has to inspect the Ward identities on a case-by-case basis. The component in the representation E is obtained by taking the linear combination $q_2\cdot$Eq. (36) $-q_1$Eq. $(36)_{q_1\to q_2\to q_3}$.

The result is

$$-q_1q_2q_3\Pi^E_{11}(q) = 2q_0q_2q_3\Pi^{T_1}_{01} - q_0q_1(q_3\Pi^{T_1}_{02} + q_2\Pi^{T_1}_{03}) \\ +q_2q_3(q_3\Pi^{T_2}_{13} + q_2\Pi^{T_2}_{12}) - q_1\Pi^{T_2}_{23}(q_2^2+q_3^2). \quad (39)$$

We note that for many actions at finite lattice spacing, the Ward identities read $\hat{q}_\mu\Pi_{\mu\nu} = 0$ with $\hat{q}_\mu \equiv 2\sin(aq_\mu/2)$. In equations (35) and (36), and in the equations in the next subsection, q_μ should then be replaced by $\hat{q}_\mu$.

3.1 Parametrization of the polarization tensor at small momenta

Of particular relevance is the behavior of the polarization tensor at very small momenta, since in infinite volume $\Pi(0)$ must be subtracted from $\Pi(Q^2)$ in order to remove a logarithmic divergence. On the torus we Taylor-expand the different contributions to the polarization tensor up to quartic order, including all the polynomials compatible with the respective cubic representations,

$$\bar{\Pi}^{T_1}_{01}(q) = q_0q_1\big[A_{T_1} + B_{T_1}\big(q_1^2 - \tfrac{3}{5}\boldsymbol{q}^2\big) \\ +C_{T_1}q_0^2 + D_{T_1}\boldsymbol{q}^2\big], \quad (40)$$

$$\bar{\Pi}^{T_2}_{12}(q) = q_1q_2\big[A_{T_2} + B_{T_2}q_0^2 + C_{T_2}\boldsymbol{q}^2 \\ +D_{T_2}\big(q_1^2+q_2^2-\tfrac{6}{7}\boldsymbol{q}^2\big)\big], \quad (41)$$

$$\bar{\Pi}^{E}_{11}(q) = A_E\big(q_1^2 - \tfrac{1}{3}\boldsymbol{q}^2\big) + B_Eq_0^2\big(q_1^2-\tfrac{1}{3}\boldsymbol{q}^2\big) \\ +C_E\big(q_1^4 - \tfrac{1}{3}\textstyle\sum_j q_j^4 - \tfrac{6}{7}\boldsymbol{q}^2(q_1^2-\tfrac{1}{3}\boldsymbol{q}^2)\big) \\ +D_E\boldsymbol{q}^2\big(q_1^2-\tfrac{1}{3}\boldsymbol{q}^2\big), \quad (42)$$

$$\bar{\Pi}^{A_1}_{11}(q) = \bar{A}q_0^2 + \bar{B}\boldsymbol{q}^2 + \bar{C}q_0^4 + \bar{D}q_0^2\boldsymbol{q}^2 \\ +\bar{E}(\boldsymbol{q}^2)^2 + \bar{F}\big(\textstyle\sum_j q_j^4 - \tfrac{3}{5}(\boldsymbol{q}^2)^2\big), \quad (43)$$

$$\hat{\Pi}^{A_1}(q) = \hat{A}q_0^2 + \hat{B}\boldsymbol{q}^2 + \hat{C}q_0^4 + \hat{D}q_0^2\boldsymbol{q}^2 \\ +\hat{E}(\boldsymbol{q}^2)^2 + \hat{F}\big(\textstyle\sum_j q_j^4 - \tfrac{3}{5}(\boldsymbol{q}^2)^2\big). \quad (44)$$

It should be noted that since the momentum variable q assumes only discrete values on the torus, one can always represent a function of q as a polynomial. Also, in infinite volume, the spectral representation (10) shows that for a spectral function admitting a mass gap, all the derivatives of the vacuum polarization exist and are finite at the origin, and that the vacuum polarization can be represented as a polynomial in Q^2 locally around the origin. Therefore one expects those coefficients in Eq. (40–44) that are commensurate with the infinite-volume tensor structure (9) to smoothly tend to a Taylor coefficient of $\Pi(Q^2)$ in the infinite-volume limit, whereas the others must vanish in the same limit. Before considering this limit however, we work out the consequences of the conservation of the current on the coefficients.

From the Ward identity (35), we can express all five series expansions in terms of two of them, by relating the coefficients. We choose $\bar{\Pi}^{T_1}$ and $\bar{\Pi}^{T_2}$ to be independent series and find for the other coefficients

$$A_E = A_{T_2}, \quad (45)$$
$$B_E = B_{T_2} - B_{T_1}, \quad (46)$$
$$C_E = 2D_{T_2}, \quad (47)$$
$$D_E = C_{T_2} - \tfrac{1}{7}D_{T_2}; \quad (48)$$

$$\bar{A} = -\tfrac{1}{4}A_{T_1}, \quad (49)$$
$$\bar{B} = \tfrac{1}{4}(A_{T_1} - \tfrac{2}{3}A_{T_2}), \quad (50)$$
$$\bar{C} = -\tfrac{1}{4}C_{T_1}, \quad (51)$$
$$\bar{D} = \tfrac{1}{4}(C_{T_1} + \tfrac{4}{15}B_{T_1} - D_{T_1} - \tfrac{2}{3}B_{T_2}), \quad (52)$$
$$\bar{E} = \tfrac{1}{4}(D_{T_1} + \tfrac{4}{105}D_{T_2} - \tfrac{2}{3}C_{T_2}), \quad (53)$$
$$\bar{F} = \tfrac{1}{4}(B_{T_1} - \tfrac{1}{3}D_{T_2}); \quad (54)$$

$$\hat{A} = -\tfrac{3}{4}A_{T_1}, \quad (55)$$
$$\hat{B} = -\tfrac{1}{4}(A_{T_1} + 2A_{T_2}), \quad (56)$$
$$\hat{C} = -\tfrac{3}{4}C_{T_1}, \quad (57)$$
$$\hat{D} = -\tfrac{1}{4}(-\tfrac{4}{5}B_{T_1} + 3D_{T_1} + C_{T_1} + 2B_{T_2}), \quad (58)$$
$$\hat{E} = -\tfrac{1}{4}(-\tfrac{4}{35}D_{T_2} + 2C_{T_2} + D_{T_1}), \quad (59)$$
$$\hat{F} = -\tfrac{1}{4}(B_{T_1} + D_{T_2}). \quad (60)$$

This exercise explicitly illustrates that two of the five introduced functions are sufficient to fully characterize the polarization tensor. In particular, the latter is known entirely once the off-diagonal components (parametrized by $\bar{\Pi}^{T_1}$ and $\bar{\Pi}^{T_2}$) are known.

In addition to the terms listed above, there are terms that are not constrained by the Ward identities, for instance

$$\Pi_{00}(0,\boldsymbol{q}) \equiv \chi(\boldsymbol{q}), \quad (61)$$

which can be interpreted as a static susceptibility. When the time extent β is infinite, we have $\chi(\boldsymbol{q}) \sim \boldsymbol{q}^2$ at small momentum, due to the presence of a mass gap in QCD, and this guarantees that the photon remains massless. When β is finite however, $\chi(\boldsymbol{0})$ is the thermal electric charge susceptibility, which does not vanish. Our parametrization so far does not allow for this effect, and we must thus add the terms

$$\bar{\Pi}^{A_1}_{11} \supset \bar{\chi}\delta_{q,0}, \qquad \hat{\Pi}^{A_1}_{11} \supset \hat{\chi}\delta_{q,0} \quad (62)$$

to the generic expressions (40–44)[3], where $\hat{\chi}$ and $\bar{\chi}$ are two new coefficients.

When some of the dimensions become infinite, non-analyticities in the momenta can appear. A familiar case is the limit where the spatial dimensions become infinite, but β remains finite. Then at small momenta, $\Pi_{00}(q) \sim \frac{\chi(\boldsymbol{0})D\boldsymbol{q}^2}{|q_0|+D\boldsymbol{q}^2}$ due to the diffusion pole (D is the electric charge diffusion constant, see [28] for a review).

[3] At finite $\boldsymbol{q}$, the coefficients $\hat{B}$ and $\bar{B}$ already capture the effect of the susceptibility $\chi(\boldsymbol{q})$.

In infinite volume, the vacuum polarization $\Pi(Q^2)$ is uniquely defined, due to the constrained Lorentz structure of the polarization tensor. On the $\beta \times L^3$ torus however, we see that there are two obvious definitions of $\Pi(0)$, one that one may extract from the T_1 representation, and one from the T_2 representation. Indeed, to quadratic order the various components read

$$\Pi_{01}(q) = A_{T_1} q_0 q_1, \tag{63}$$
$$\Pi_{12}(q) = A_{T_2} q_1 q_2, \tag{64}$$
$$\Pi_{11}(q) = (\bar{\chi} + \hat{\chi})\delta_{q,0} + A_{T_2} q_1^2 - (A_{T_1} q_0^2 + A_{T_2} \boldsymbol{q}^2), \tag{65}$$
$$\Pi_{00}(q) = (\hat{\chi} - 3\bar{\chi})\delta_{q,0} - A_{T_1} \boldsymbol{q}^2. \tag{66}$$

Disregarding the susceptibility terms, they thus have the form (9) expected in infinite volume, except for Π_{11} if $q_1^2 \neq \boldsymbol{q}^2$. In general however $A_{T_1} \neq A_{T_2}$, and one has to specify how the extrapolation to $q = 0$ is done. The vacuum polarization extracted from the component $\Pi_{00}(Q)$ is the same as the one extracted from Π_{01}, but one must be careful with Π_{11}, given that the tensor structure appearing in Eq. (65) is not the one expected in infinite volume unless $A_{T_1} = A_{T_2}$.

The equalities (45) to (60) can be used to test computer programs. Once these tests are passed, a number of checks for finite-volume effects can be made. Apart from $A_{T_1} \stackrel{?}{=} A_{T_2}$, one can check for instance whether B_{T_1} vanishes and $C_{T_1} \stackrel{?}{=} D_{T_1}$, as one expects in infinite volume, and similarly in the T_2 channel.

Finally we note that if one calculates the isospin current correlator and introduces twisted boundary conditions for the quarks fields (see for instance [6] and Refs. therein), then the cubic symmetry is in general broken down even further, and the analysis above should be adapted accordingly.

3.2 A sum rule for the finite-volume spectral function

The Ward identities $k_\mu \Pi_{\mu\nu} = 0$ imply

$$k_3 \Pi_{33}(k) = 0, \qquad k = (0, 0, 0, k_3). \tag{67}$$

This relation holds both in finite and in infinite volume. We now want to turn it into a sum rule for the spectral function ρ_{33} (introduced in Eq. 2) via the dispersion relation for the Euclidean correlator. The spectral function associated with the spatial current correlator Π_{33} grows as k_0^2 at large frequencies. Therefore a subtraction is necessary to obtain a convergent sum rule. Taking the difference between the finite-volume and the infinite volume correlator leads to a subtracted spectral function $\propto k_0^{-2}$ at large frequencies, due to the absence of operators of dimension less than 4 in the operator product expansion of $\Pi_{\mu\nu}$. If $\Delta\rho_{33}$ is the difference between the finite-volume spectral function and the infinite-volume one, the spectral representation

$$\Pi_{33}(k_3, \beta, L) - \Pi_{33}(k_3, \infty, \infty) = \int_{-\infty}^{\infty} \frac{d\omega}{\omega} \Delta\rho_{33}(\omega, k_3, \beta, L) \tag{68}$$

is thus convergent[4]. The Ward identity (67) can then be writen

$$k_3 \int_{-\infty}^{\infty} \frac{d\omega}{\omega} \Delta\rho_{33}(\omega, k_3, \beta, L) = 0. \tag{69}$$

For $k_3 \neq 0$, this sum rule constrains the finite-volume alterations of the spectral density relative to the infinite-volume situation. It may be useful in the finite-temperature context, where one wants to determine the distribution of the spectral weight $\Delta\rho_{33}(\omega, k_3, \beta, L)$, see [28] and references therein. If one takes the spatial volume to infinity, k_3 can be made as small as desired and the sum rule for $\Delta\rho_{33}$ then also holds for $k_3 = 0$. We note that the sum rule (69) is simpler in QCD than in the $\mathcal{N} = 4$ super Yang-Mills theory, because in the latter case the contribution of the scalar fields to the current contains a derivative, which means that the the current itself is not invariant under a local symmetry transformation, and this leads to a contact term in the current correlator [29].

4 Computational strategies for $\Delta\alpha(Q^2)$ and a_μ^{HLO}

In lattice QCD it is customary to work with correlation functions which are functions of Euclidean time t and spatial momentum $\boldsymbol{k}$. This representation has the advantage that the low-lying states dominate exponentially at large t. Here we first consider the situation in infinite volume, deriving the relation between the Euclidean correlator and the spectral function $\rho(q^2)$ introduced in Eq. (3). In the next section we show that a_μ can be calculated in terms of the $(t, \boldsymbol{k})$-dependent correlator using a different kernel[5]. We propose a way of treating different intervals of t differently when computing a_μ, combining the Euclidean-space calculation with the low-energy part of the spectral function.

4.1 The pion form factor in the timelike region

The pion form factor in the timelike region can in principle be calculated based on Eq. (7) in the threshold region,

$$2m_{\pi^\pm} \leq \sqrt{s} \leq 2\big(m_{\pi^\pm} + m_{\pi^0}\big). \tag{70}$$

Via Eq. (5), it can directly be compared to the experimental results for the R ratio (for a precision comparison, care must be taken of QED corrections). The quality of the experimental data can be viewed in Fig. (3) of Ref. [19]. A further constraint on this region comes from the fact that the form factor $F_\pi(s)$ admits a convergent Taylor expansion in s with a radius given by the parameters of the ρ meson, (m_ρ, Γ_ρ). The first two terms are well constrained by the pion form factor in the spacelike region,

$$F_\pi(s) = 1 + \tfrac{1}{6} r_\pi^2 \cdot s + \mathrm{O}(s^2). \tag{71}$$

[4] We have written Π and ρ as functions of the momentum variables that do not vanish.

[5] H.M. is indebted to Andreas Jüttner for bringing to his attention coordinate space methods for the calculation of a_μ.

This means that calculating the pion radius in lattice QCD also helps to constrain/check the spectral function in the threshold region. Although the region (70) only accounts for about 10% of the total $a_\mu^{\rm HLO}$, it is still important to control its contribution at the level of a few percent in preparation for the upcoming $(g-2)_\mu$ experiment at Fermilab [30].

This program would be a relatively modest but certainly valuable contribution of lattice QCD to the precision determination of $\Delta\alpha(M_Z^2)$ and $a_\mu^{\rm HLO}$.

4.2 Mixed-representation correlator

We consider the positive-definite correlator[6]

$$G(t) \equiv \int \mathrm{d}\boldsymbol{x}\, \langle j_z^{\rm em}(t,\boldsymbol{x}) j_z^{\rm em\,\dagger}(0)\rangle. \tag{72}$$

We will now derive a spectral representation for $G(t)$ in terms of the spectral function $\rho(q^2)$ of Eq. (3). To this end, we note that the correlator $G(t)$ can also be obtained from $\Pi_{\mu\nu}(q)$ by Fourier transformation,

$$G(t) = -\int_{-\infty}^{\infty} \frac{\mathrm{d}\omega}{2\pi} \Pi_{zz}(\omega, \boldsymbol{k}=0)\, e^{i\omega t}. \tag{73}$$

Now, the tensor structure (9) implies

$$\Pi_{zz}(\omega, \boldsymbol{k}=0) = -\omega^2 \Pi(\omega^2), \tag{74}$$

and secondly we can substitute the dispersion relation (10) into Eq. (73). Noting that the $\Pi(0)$ term only contributes for $t=0$, we obtain for $t\neq 0$

$$G(t) = \int_{-\infty}^{\infty} \frac{\mathrm{d}\omega}{2\pi} \omega^4 \int_0^\infty \mathrm{d}s \frac{\rho(s)}{s(s+\omega^2)}\, e^{i\omega t}. \tag{75}$$

The integral is easily carried out and one obtains (again for $t\neq 0$),

$$G(t) = \frac{1}{2}\int_0^\infty \mathrm{d}s\, \sqrt{s}\rho(s) e^{-\sqrt{s}|t|} \tag{76}$$

$$= \int_0^\infty \mathrm{d}\omega\, \omega^2 \rho(\omega^2) e^{-\omega|t|}. \tag{77}$$

Eq. (77) is the sought after spectral representation. One can of course derive the spectral representation of the correlator with non-vanishing spatial momentum,

$$\int \mathrm{d}\boldsymbol{x}\, e^{-i\boldsymbol{k}\cdot\boldsymbol{x}} \langle j_z(t,\boldsymbol{x}) j_z^\dagger(0)\rangle \tag{78}$$

$$= \int_{|\boldsymbol{k}|}^\infty \mathrm{d}\omega\, (\omega^2 - \boldsymbol{k}^2 + k_z^2)\, \rho(\omega^2 - \boldsymbol{k}^2) e^{-\omega|t|}.$$

Using the same parametrization of the phenomenological $R(s)$ ratio as in section (2.1), we obtain the dimensionless correlator $t^3 G(t)$ pictured in Fig. (6). Beyond say 2fm, it falls off rapidly to zero, asymptotically as $e^{-2m_\pi t}$. We note that experimental data has been used before to 'predict' the form of the configuration-space Euclidean correlator in the context of holographic models [31].

One can invert the Fourier transform (73), and express the vacuum polarization (74) through the mixed-representation correlator,

$$\Pi(\omega^2) = \frac{1}{\omega^2}\int_{-\infty}^\infty \mathrm{d}t\, e^{-i\omega t} G(t). \tag{79}$$

At small ω, the vacuum polarization behaves as

$$\Pi(\omega^2) \overset{\omega\to 0}{\sim} \frac{1}{\omega^2}\int_{-\infty}^\infty \mathrm{d}t\, G(t) - \frac{1}{2}\int_{-\infty}^\infty \mathrm{d}t\, t^2 G(t) + \ldots \tag{80}$$

The $\frac{1}{\omega^2}$ term vanishes, as the corresponding integral represents the quark number susceptibility of the vacuum (if one thinks of z as the 'time' direction). Thus

$$\Pi(\omega^2) - \Pi(0) = \int_{-\infty}^\infty \mathrm{d}t\, G(t) \left[\frac{e^{-i\omega t}-1}{\omega^2} + \frac{t^2}{2}\right]. \tag{81}$$

This integral is UV-finite by power counting (leaving in the term $\int \mathrm{d}t G(t) = 0$ makes this explicit). We also note that $G(t)$ is an even function of t, so that the expression is real, and we can write

$$\Pi(\omega^2) - \Pi(0) = 2\int_0^\infty \mathrm{d}t\, G(t)\Big[\frac{t^2}{2} - \frac{1-\cos\omega t}{\omega^2}\Big] \tag{82}$$

$$= \frac{1}{\omega^2}\int_0^\infty \mathrm{d}t\, G(t)\Big[\omega^2 t^2 - 4\sin^2(\tfrac{1}{2}\omega t)\Big]. \tag{83}$$

The leading hadronic contribution to the anomalous magnetic moment of the muon can be expressed through the vacuum polarization $\Pi(Q^2)$, Eq. (12 and 14). Using relation (83), we can write $a_\mu^{\rm HLO}$ as

$$a_\mu^{\rm HLO} = 4\alpha^2 m_\mu \int_0^\infty \mathrm{d}t\, t^3\, G(t)\, \tilde{K}(t), \tag{84}$$

$$\tilde{K}(t) \equiv \frac{2}{m_\mu t^3}\int_0^\infty \frac{\mathrm{d}\omega}{\omega}\, K_E(\omega^2)\left[\omega^2 t^2 - 4\sin^2\left(\tfrac{\omega t}{2}\right)\right]. \tag{85}$$

The kernel $\tilde{K}(t)$ is dimensionless, proportional to t at small t and to $1/t$ at large t. The factor t^3 was chosen because $t^3\, G(t)$ is dimensionless and finite as $t\to 0$. The integrand of Eq. (84) is displayed in Fig. (4).

4.3 Euclidean correlator vs. the R ratio

We have already confronted the vacuum polarization calculated on the lattice to the $R(s)$ ratio via the dispersion relation in section (2.1). Here we propose to do the same in the mixed $(t,\boldsymbol{k})$ representation. This has the advantage that the correlator involves only on-shell states. In addition, the continuum limit is approached with $\mathrm{O}(a^2)$ corrections (assuming the vector current is improved).

[6] In Minkowski space, the field operators $\hat{j}_\mu$ are hermitian, $\hat{j}_\mu^\dagger = j_\mu$. In Euclidean space, while $\hat{j}_0^\dagger = \hat{j}_0$, the spatial current is antihermitian $\hat{j}_z^\dagger = -\hat{j}_z$.

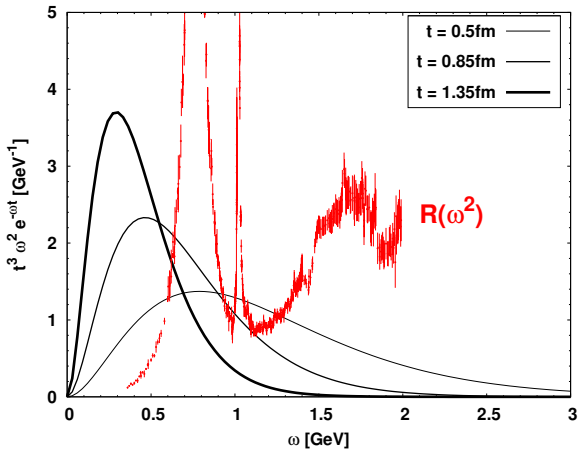

Fig. 3: The kernel of the spectral representation (77) for three different Euclidean times, and the experimental $R(\omega^2)$ ratio up to $\omega = 2$GeV [15].

Consider the correlator $G(t)$, it is related to the spectral function $\rho(\omega^2)$ via Eq. (77). Depending on the value of t, the Euclidean correlator $G(t)$ is sensitive to different energy intervals $\Delta\omega$. This simple fact is illustrated in Fig. (3). Confronting in this way the value of $G(t)$ calculated on the lattice with the phenomenological value offers a way for the lattice practitioner to test the validity of the $R(s)$ parametrization. Of course this test will only be useful if the correlator, as well as its statistical and systematic error, are accurately determined. This also means that the chiral extrapolation, if any, must be under good control. Choosing t between 0.5 and 1.5fm yields sensitivity to the region most relevant to the muon anomalous magnetic moment, encompassing in particular the ρ, ω and ϕ resonances. The comparison can therefore provide a useful test of the correctness of the phenomenological approach.

4.4 Combining spacelike and timelike correlators

There are many scales entering the integral (84) yielding $a_\mu^{\rm HLO}$. The most relevant ones are the lepton mass m_μ, the pion mass m_π, the box size L and the integration variable t. An advantage of working in the mixed $(t, \boldsymbol{k})$ representation is that a Hamiltonian interpretation of the expression is straightforward. This motivates us to separate the contribution of different t-intervals to the integral (84) in the following way. We write the integral as a sum of three terms,

$$a_\mu^{\rm HLO} = a_\mu^<(t_0, L) + \Delta a_\mu(t_0, t_1, L) + a_\mu^>(t_1, L), \qquad (86)$$

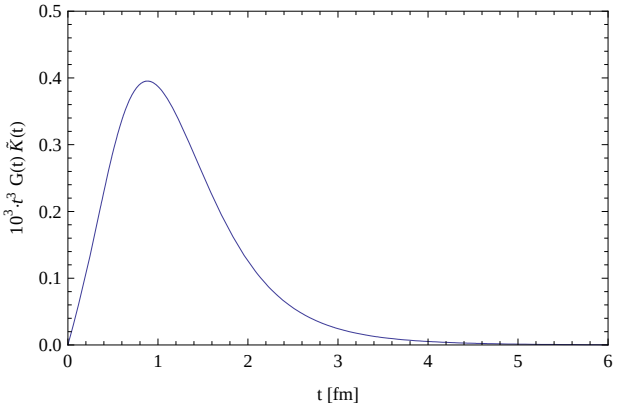

Fig. 4: The integrand of Eq. (84) in infinite volume, obtained from the phenomenological parametrization (18) of the $R(s)$ ratio.

with

$$a_\mu^<(t_0, L) \equiv 4\alpha^2 m_\mu \int_0^{t_0} {\rm d}t\, t^3\, G(t)\, \tilde{K}(t) \qquad (87)$$

$$\Delta a_\mu(t_0, t_1, L) \equiv 4\alpha^2 m_\mu \int_{t_0}^{t_1} {\rm d}t\, t^3\, G(t)\, \tilde{K}(t). \qquad (88)$$

$$a_\mu^>(t_1, L) \equiv 4\alpha^2 m_\mu \int_{t_1}^{\infty} {\rm d}t\, t^3\, G(t)\, \tilde{K}(t). \qquad (89)$$

The short-distance contribution $a_\mu^<(t_0) \equiv \lim_{L\to\infty} a_\mu^<(L, t)$ can be calculated in perturbation theory; the perturbative series is known to have good convergence properties in the vector channel. For the purpose of calculating a_μ, the practical question will be whether there is a choice of t_0 where the perturbative series shows good convergence *and* the discretization errors are small[7].

A state of energy E makes a contribution of order e^{-Et_1} to $a_\mu^>(t_1, L)$. With a solid understanding of the low-energy spectrum, one can therefore analyze this contribution for large enough t_1 and in particular its finite-volume effects. The larger t_1, the stronger low-energy states dominate, but on the other hand the numerical importance of this contribution is reduced. Therefore one would like to choose t_1 as small as possible while the contribution is still dominated by the analytically tractable low-lying states.

In appendix (A) we show that the finite-size correction on the contribution coming from $\rho(s < 4(m_{\pi_\pm} + m_{\pi_0})^2)$ to the long-distance part of the correlator is large (by long-distance, we mean $t \gg (2m_\pi)^{-1}$ and $t \gg L/\pi$). Figure (5) illustrates that this contribution represents 50% of the full correlator starting at $t \approx 2.9$fm. The contribution of $G(t \geq 2.9\text{fm})$ to $a_\mu^{\rm HLO}$ is modest (see Fig. 4), but certainly not negligible if one aims at a precision at the percent level or better on $a_\mu^{\rm HLO}$.

In view of these finite-size corrections, it appears preferable to treat the contribution $a_\mu^>(t_1)$ differently, if t_1 is

[7] An analogous issue arises when computing a_μ in four-momentum space, where perturbation theory is found to match the lattice vacuum polarization down to about 3GeV^2 [4].

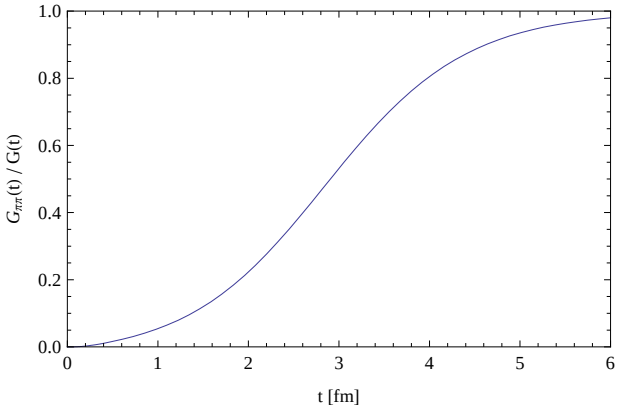

Fig. 5: The fraction of the $\boldsymbol{q} = 0$ Euclidean current correlator $G(t)$ coming from the region $2m_{\pi^\pm} \leq \sqrt{s} < 2(m_{\pi^\pm} + m_{\pi^0})$ of the spectral function (in infinite spatial volume). See Eq. (77).

chosen large. Eq. (121) is an exact spectral representation of this contribution. The infinite-volume spectral function $\rho(\omega^2)$ can be calculated on the lattice below the four-pion threshold via Eq. (6, 7). Therefore, if the states below the four-pion threshold saturate the current correlator beyond t_1, $a_\mu^>(t_1)$ can be obtained from first principles through Eq. (121), while Δa_μ is calculated by integrating the Euclidean correlator as in (88). This is an example of the potentially powerful interplay of a correlator in the spacelike and in the timelike region. The difficulty with this strategy is that numerically, the saturation at (say) the 95% level by the states below the four-pion threshold only begins around 5.3fm, at which point the contribution to $a_\mu^{\rm HLO}$ is already extremely small. Choosing t_1 as large as 5.3fm is therefore not a very attractive option. The strategy of splitting up $a_\mu^{\rm HLO}$ into three contributions and using the spectral representation for the long-distance part would become more attractive if one could determine the spectral function up to somewhat higher energies, but the formalism has not yet been developed to handle the mixing of two-pion with four-pion states.

The analysis outlined above shows that the relative finite-size effects on the long-distance contributions to the vacuum polarization and to $a_\mu^{\rm HLO}$ are large. Fortunately, the size of these contributions is small (albeit non-negligible) compared to the total $a_\mu^{\rm HLO}$. The finite-size effects associated with the higher-lying states remains however unknown, and it should be investigated.

5 A new reference scale for lattice QCD

When making predictions for hadronic observables in lattice QCD, a mandatory step is to calibrate the length of the lattice spacing a in physical units (fm). In principle, calculating the proton mass M_p in lattice units, and equating it to 938.272MeV yields the desired value. However, the proton mass is difficult to calculate accurately on the lattice at light quark masses, and in practice one chooses a different dimensionful quantity to 'set the scale'. It is however not easy to come up with a quantity which is both accurately calculable on the lattice and accurately extracted from experiment[8]. A quantity that has proved very useful is the Sommer reference scale r_0, defined from the static quark potential [32]. While it is accurately calculable on the lattice, its value in the real world is not known precisely, since its extraction from the upsilon spectrum requires introducing a potential model. This procedure leads to a certain degree of ambiguity (up to $\sim 8\%$, to be conservative).

Here we propose a new reference scale τ_0 based on the vector current correlator, which we believe satisfies the requirement of being accurately calculable. Given the level of experimental effort that has gone into the measurement of the $R(s)$ ratio particularly in the past decade, we believe that the value of τ_0 can also accurately be extracted from the compiled data of e^+e^- annihilation experiments. Figure (6) displays the electromagnetic current correlator $G(t)$ obtained from our simple parametrization of the R ratio, Eq. (18).

At long time separations (somewhere beyond 1fm), the vector channel correlator becomes noisy in Monte-Carlo simulations. At short distances, one is confronted with cutoff effects from the lattice, and secondly, QCD is approximately scale-invariant, so that the sensitivity to the confinement scale is low. This dictates that one should choose a reference time-scale somewhere between 0.5fm and 1fm.

Another computational aspect is that it is significantly easier to calculate correlators in channels where no Wick-disconnected diagrams appear. With the commonly used statistical sampling methods, connected diagrams exhibit better signal-to-noise ratios. The correlator of the electromagnetic current will contain the difference of the strange-quark disconnected loops and the light-quark disconnected loop. Therefore, for the purpose of statistical accuracy it is preferable to use the isospin current, in which disconnected diagrams cancel out (assuming exact isospin symmetry). On the phenomenological side, this means that one should only include those final states with isospin $I = 1$ in the evaluation of the R-ratio. We therefore define

$$R_1(s) \equiv \frac{\sigma(e^+e^- \to \text{hadrons} \,|\, I = 1)}{4\pi\alpha(s)^2/(3s)}. \qquad (90)$$

In particular, the bulk of the ω contribution, which decays into an $I = 0$ three-pion state, should not be included; nor should the ϕ meson be included. The bulk of the low-energy isospin-current spectral function will thus come from the two-pion channel. The restriction to $I = 1$ final states can be done in a model-independent way as long as isospin breaking effects in QCD are negligible to the desired degree of accuracy. The number of open channels between 1.4GeV and 2.0GeV increases rapidly, and above 2GeV, practically only inclusive measurements are made. Therefore it is preferable to suppress the high-energy region by choosing a relatively large τ_0.

[8] If the goal is only to calibrate the *relative* size of two lattice spacings, the second requirement is not mandatory.

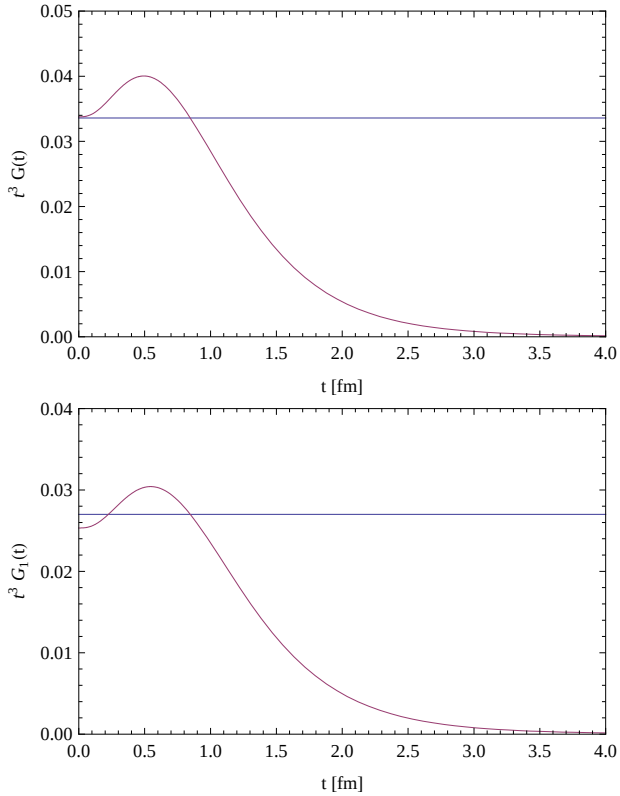

Fig. 6: Top: the correlator of the electromagnetic current $j_z^{\rm em}$ at zero spatial momentum in infinite volume obtained from the phenomenological parametrization of the $R(s)$ ratio. Bottom: the same for its isospin component j_z^I.

We thus define the Euclidean correlator $G_1(t)$ analogously to $G(t)$ (Eq. 72), but replacing the electromagnetic current $j_\mu^{\rm em}$ by its isospin component

$$j_\mu^I = \tfrac{1}{2}(\bar{u}\gamma_\mu u - \bar{d}\gamma_\mu d). \tag{91}$$

We define the time scale τ_0 by the equation

$$\tau_0^3\, G_1(\tau_0) \stackrel{\rm def}{=} 0.027. \tag{92}$$

Figure (6) displays the electromagnetic current correlator $G(t)$ obtained from our simple parametrization of the R ratio, Eq. (18), as well as the corresponding isospin current correlator $G_1(t)$ based on the model

$$\begin{aligned} R_1(s) = {} & \theta(\sqrt{s} - 2m_{\pi^\pm})\;\theta(4.4m_{\pi^\pm} - \sqrt{s}) \\ & \times \tfrac{1}{4}\Big[1 - \tfrac{4m_{\pi^\pm}^2}{s}\Big]^{3/2}\big(0.6473 + f_0(\sqrt{s})\big) \\ & + \theta(\sqrt{s} - 4.4m_{\pi^\pm})\theta(M_3 - \sqrt{s}) f_1(\sqrt{s}) \\ & + 3\big((\tfrac{1}{2})^2 + (\tfrac{1}{2})^2\big)\;\theta(\sqrt{s} - M_3). \end{aligned} \tag{93}$$

(the values used for the parameters are those in table 1). Based on this approximate form of the spectral function, we find

$$\tau_0 \simeq 0.85\text{fm}. \tag{94}$$

We postpone a more accurate phenomenological evaluation of τ_0 and its uncertainty to a future publication. At a practical level, a nice feature of the τ_0 definition is that no derivative must be taken and no fit need be performed, one will 'merely' have to perform an interpolation to the point τ_0.

Of course, many reference scales can be defined in a similar way. As a slight variation of the definition (92), one could also use the time component of the current with a non-vanishing spatial momentum $\boldsymbol{k}$. The advantage is that the correlator does not vary as fast at short distances, only as $\boldsymbol{k}^2/t$ instead of $1/t^3$. The spectral representation then reads[9]

$$\begin{aligned} & \int {\rm d}\boldsymbol{x}\, e^{-i\boldsymbol{k}\cdot\boldsymbol{x}}\, \langle j_0(t,\boldsymbol{x}) j_0(0)\rangle \\ & \qquad = \boldsymbol{k}^2 \int_{|\boldsymbol{k}|}^\infty {\rm d}\omega\; \rho(\omega^2 - \boldsymbol{k}^2) e^{-\omega|t|}. \end{aligned} \tag{95}$$

A reference scale based on this correlator might be an attractive alternative depending on its signal-to-noise ratio.

If one manages to calculate the disconnected diagrams accurately, then a definition based on the electromagnetic current could become more attractive. For instance, defining $\tau_{\rm em}^3 G(\tau_{\rm em}) \stackrel{\rm def}{=} 0.0336$ leads again, using Eq. (18), to $\tau_{\rm em} \approx 0.85$. This has the advantage that the selection of unit-isospin final states in the $R(s)$ ratio is not required, nor is the assumption of exact isospin symmetry.

6 Lüscher formula with twisted boundary conditions

For the evaluation of formula (7) the scattering phase shift δ_1 of the $I = l = 1$ channel must be known as a function to obtain its derivative. Lüscher showed precisely [14] how individual values of the scattering phase can be reconstructed out of the two particle energy spectrum inside a finite volume. The problem that arises is that in practice, for a given volume size, only a few values of the scattering phase shift can be reconstructed. If the scattering phase shift is needed as a function of momentum the computational cost increases rapidly since the results of many simulations with different volume have to be combined. Rummukainen and Gottlieb [33] showed that by extending the formalism to non vanishing center of mass momenta more points of the scattering phase shift can be extracted per volume. A further generalization is the use of twisted boundary conditions that introduce a new continuous parameter, the twist angle, to the simulations. The twist angle can then be used to modify the momentum almost continuously and therefore enables one to "scan" the scattering phase shifts. The derivation of the extended version of the Lüscher formula closely follows the original one in [14] and is therefore only sketched here. First we introduce the wave function in infite volume. It describes two bosons of equal mass, and obeys the Schrödinger equation

$$\left[\frac{\boldsymbol{p}^2}{2\mu} + V(|\boldsymbol{r}|)\right]\Psi(\boldsymbol{r}) = E\,\Psi(\boldsymbol{r}) \tag{96}$$

[9] It is easily obtained from Eq. (78) by using the Ward identity $\partial_\mu j_\mu = 0$.

where the potential $V(|\boldsymbol{r}|)$ is spherically symmetric and has a finite range R. The wave function can be extended into spherical harmonics with its radial components satisfying the radial Schrödinger equation

$$\left[\frac{d^2}{dr^2}+\frac{2}{r}\frac{d}{dr}-\frac{l(l+1)}{r^2}+k^2-2\mu V(r)\right]\Psi_{lm}(r)=0. \quad (97)$$

In the region where the potential vanishes, the solution is given by $\Psi_{lm}(r)=\alpha_l(k)j_l(kr)+\beta_l(k)n_l(kr)$, where the constants α_l and β_l determine the scattering phase shifts via

$$e^{2i\delta_l(k)}=\frac{\alpha_l(k)+i\beta_l(k)}{\alpha_l(k)-i\beta_l(k)}. \quad (98)$$

We now enclose both particles in a box of size $L\times L\times L$ and impose twisted boundary conditions

$$\Psi(\boldsymbol{r}+\boldsymbol{n}L)=e^{i\boldsymbol{n}\cdot\boldsymbol{\phi}}\Psi(\boldsymbol{r}), \quad (99)$$

where the triplet $\boldsymbol{\phi}$ of twist angles was introduced. The potential must also be replaced by a periodic version

$$V_L(\boldsymbol{r})=\sum_{\boldsymbol{n}\in\mathbb{Z}^3}V(|\boldsymbol{r}+\boldsymbol{n}L|). \quad (100)$$

Inside the box the energy spectrum is now discrete, with the energy-momentum relation still given by $E=k^2/2\mu$. As in the periodic case, the Schrödinger equation in the region of vanishing potential Ω reduces to the Helmholtz equation,

$$(\Delta+k^2)\Psi(\boldsymbol{r})=0. \quad (101)$$

In this outer region Ω the eigenfunctions of the Hamiltonian now have to be solutions of the Helmholtz equation, that are expandable in spherical harmonics and have radial components

$$\Psi_{lm}(r)=b_{lm}\big(\alpha_l(k)j_l(kr)+\beta_l(k)n_l(kr)\big). \quad (102)$$

According to a theorem by Lüscher (proof given in appendix A of [14]) for each solution of the Helmholtz equation in Ω that can be expanded in this way there exists a unique eigenfunction of the Hamiltonian that matches this solution in Ω. Finding the general solution of the Helmholtz equation therefore suffices for determining the formula for the scattering phase shifts.

To simplify the derivation a bit, the momenta of the solutions of the Helmholtz equation are now assumed not to belong to the singular set $\Gamma_s=\left\{k\in\mathbb{R}\,\middle|\,k=\pm\frac{2\pi}{L}|\boldsymbol{n}|,\text{ for }\boldsymbol{n}\in\mathbb{Z}^3\right\}$. Momenta in this set would allow plane waves as solutions of the Helmholtz equation, which would complicate the derivation a bit. For the following steps an angular momentum cutoff Λ is introduced, so that only the partial waves with an angular momentum smaller or equal to Λ feel the presence of the potential.

The solutions we are about to construct should satisfy two conditions. First they have to satisfy the twisted boundary conditions (99), and second they should be bounded by a power of r^{-1} near the origin

$$\lim_{r\to 0}|r^{\Lambda+1}\Psi(\boldsymbol{r})|<\infty. \quad (103)$$

The ansatz for finding the general solution is now the Greens function

$$G^{\phi}(\boldsymbol{r};k^2)=L^{-3}\sum_{\boldsymbol{p}\in\Gamma^{\phi}}\frac{e^{i\,\boldsymbol{p}\cdot\boldsymbol{r}}}{p^2-k^2} \quad (104)$$

where the momenta are elements of $\Gamma^{\phi}=\left\{\boldsymbol{p}\in\mathbb{R}^3\,\middle|\,\boldsymbol{p}=\frac{2\pi}{L}\boldsymbol{n}+L^{-1}\boldsymbol{\phi},\ \boldsymbol{n}\in\mathbb{Z}^3\right\}$. That this function satisfies the twisted boundary conditions can be shown straightforwardly, and it is also a solution of the Helmholtz equation for $\boldsymbol{r}\neq 0\,(\mathrm{mod}\,L)$. By comparison with the spherical Bessel functions one finds the behaviour of $G^{\phi}(\boldsymbol{r};k^2)$ near the origin to be

$$G^{\phi}(\boldsymbol{r};k^2)=\frac{k}{4\pi}n_0(kr)+\hat{G}^{\phi}(\boldsymbol{r};k^2) \quad (105)$$

where $\hat{G}^{\phi}(\boldsymbol{r};k^2)$ is the regular part. Further solutions may be constructed by using the function $\mathcal{Y}_{lm}(\boldsymbol{x})=r^lY_{lm}(\theta,\phi)$ to obtain the derivatives

$$G^{\phi}_{lm}(\boldsymbol{r};k^2)=\mathcal{Y}_{lm}(\boldsymbol{\nabla})G^{\phi}(\boldsymbol{r};k^2). \quad (106)$$

One can then show that the $G^{\phi}_{lm}(\boldsymbol{r};k^2)$ form a complete, normal basis of the solutions of the Helmholtz equation. Therefore the solutions that were searched for can be constructed as a linear combination of the $G^{\phi}_{lm}(\boldsymbol{r};k^2)$

$$\Psi(\boldsymbol{r})=\sum_{l=0}^{\Lambda}\sum_{m=-l}^{l}v_{lm}G^{\phi}_{lm}(\boldsymbol{r};k^2). \quad (107)$$

Like in Lüscher's paper these solutions now have to be expanded in spherical harmonics and this form has to be compared to the expansion containing the spherical Bessel functions. The expansion is similar to the one with periodic boundary conditions

$$\begin{aligned}G^{\phi}_{lm}(\boldsymbol{r};k^2)=&\frac{(-1)^l k^{l+1}}{4\pi}\Big\{n_l(kr)Y_{lm}(\theta,\phi)\\&+\sum_{l'=0}^{\infty}\sum_{m'=l'}^{l'}\mathcal{M}^{\phi}_{lm,l'm'}\big(q(k)\big)j_{l'}(kr)Y_{l'm'}(\theta,\phi)\Big\},\end{aligned} \quad (108)$$

where $q=\frac{kL}{2\pi}$ and $\mathcal{M}^{\phi}_{lm,l'm'}\big(q(k)\big)$ is given by

$$\mathcal{M}^{\phi}_{lm,l'm'}(q)=\frac{(-1)^l}{\pi^{3/2}}\sum_{j=|l-l'|}^{l+l'}\sum_{s=-j}^{j}\frac{i^j}{q^{j+1}}C_{lm,js,l'm'}\mathcal{Z}^{\phi}_{js}(1;q^2). \quad (109)$$

While the coefficients $C_{lm,js,l'm'}$ are given in [14] and can easily be calculated for a given set of indices, the Zeta-functions $\mathcal{Z}^{\phi}_{lm}(1;q^2)$ (defined below) need to be determined numerically. From the comparison of the expansions one finds (for the choice $\boldsymbol{\phi}=(\phi,\phi,\phi)$ so as not to break the cubic symmetry) the usual Lüscher formula

$$\det\left[e^{2i\delta}-\frac{\mathbf{M}^{\phi}(\mathcal{R})+i}{\mathbf{M}^{\phi}(\mathcal{R})-i}\right]=0 \quad (110)$$

where now the $\mathbf{M}^\phi$ are determined by a different Zeta-function. This formula is already the reduced one that was obtained by projecting on one of the irreducible representations ($\mathcal{R} = A_1^\pm, A_2^\pm, E^\pm, T_1^\pm, T_2^\pm$) of the cubic group, as is described in [14]. The remaining task now is to calculate the Zeta-functions $\mathcal{Z}_{lm}^\phi(s;q^2)$ that are defined by

$$\mathcal{Z}_{lm}^\phi(s;q^2) = \sum_{\boldsymbol{r}\in\tilde{\Gamma}^\phi} \mathcal{Y}_{lm}(\boldsymbol{r})(\boldsymbol{r}^2-q^2)^{-s} \tag{111}$$

for $\mathrm{Re}\, s > 1$, with $\tilde{\Gamma}^\phi = \left\{\boldsymbol{r}\in\mathbb{R}^3 \middle| \boldsymbol{r} = \boldsymbol{n} + (2\pi)^{-1}\boldsymbol{\phi},\, \boldsymbol{n}\in\mathbb{Z}^3\right\}$. Like in Lüschers original work the Zeta-functions are best calculated numerically using integral representations of the form

$$\begin{aligned}\mathcal{Z}_{lm}^\phi(1;q^2) = &\sum_{\substack{|\boldsymbol{r}|<\lambda\\ \boldsymbol{r}\in\tilde{\Gamma}^\phi}} \mathcal{Y}_{lm}(\boldsymbol{r})(\boldsymbol{r}^2-q^2)^{-1}\\ &+ (2\pi)^3\int_0^\infty dt\left[e^{tq^2}\mathcal{H}_{lm}^{\phi,\lambda}(t,0) - \frac{\delta_{l0}\delta_{m0}}{(4\pi)^2 t^{3/2}}\right].\end{aligned} \tag{112}$$

Here the reduced heat-kernel $\mathcal{H}_{lm}^{\phi,\lambda}(t,\boldsymbol{x})$ of the Laplace operator on a torus with twisted boundary conditions of size $L = 2\pi$ appears, and λ must be chosen so that $\lambda^2 > \mathrm{Re}\, q^2$. Depending on the value of t the heat kernel has two different representations based on

$$\begin{aligned}\mathcal{H}^\phi(t,\boldsymbol{x}) &= (4\pi t)^{3/2}\sum_{\boldsymbol{n}\in\mathbb{Z}^3} e^{i\boldsymbol{n}\cdot\boldsymbol{\phi}} e^{-\frac{1}{4t}(\boldsymbol{x}-2\pi\boldsymbol{n})^2}\\ &= (2\pi)^{-3}\sum_{\boldsymbol{r}\in\tilde{\Gamma}^\phi} e^{i\boldsymbol{r}\cdot\boldsymbol{x}-t\boldsymbol{r}^2},\end{aligned} \tag{113}$$

the first converges for $t \le 1$ and the second one for $t \ge 1$. With those two representations the reduced version of the heat-kernel that is needed for the integral representation of the Zeta-function can then be defined by

$$\begin{aligned}\mathcal{H}_{lm}^{\phi,\lambda}(t,\boldsymbol{x}) = (-i)^l\mathcal{Y}_{lm}(\boldsymbol{\nabla})\Big[&\mathcal{H}^\phi(t,\boldsymbol{x})\\ &- (2\pi)^{-3}\sum_{\substack{|\boldsymbol{r}|<\lambda\\ \boldsymbol{r}\in\tilde{\Gamma}^\phi}} e^{i\boldsymbol{r}\cdot\boldsymbol{x}-t\boldsymbol{r}^2}\Big].\end{aligned} \tag{114}$$

Using for instance the program *Mathematica* the Zeta-function can then be calculated numerically.

Figure 7 illustrates the advantage of using the twisted boundary conditions. For a simple quantum mechanical example with a potential well (see appendix B) the reconstructed scattering phase shift $\delta_1(k)$ is shown. Fig. 7a shows the scattering phase shift reconstructed using periodic boundary conditions and several volumes, while for fig. 7b twisted boundary conditions were used. In the second figure the volume was set to be $L = 20$, while the twist angle ranges between $\phi = 0$ and $\phi = 0.4$. In both figures the blue curve is the scattering phase shift calculated in infinite volume that was added as a comparison to the numerically calculated data. This simple example already

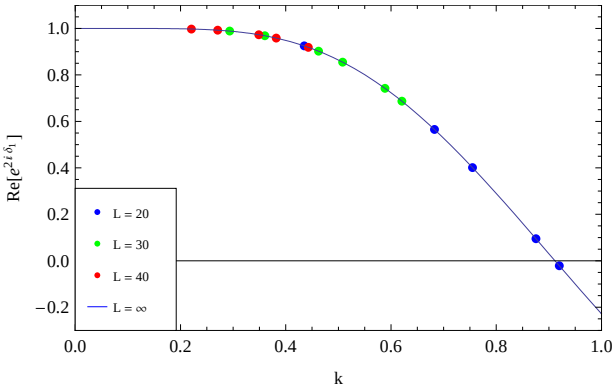

(a) periodic boundary conditions

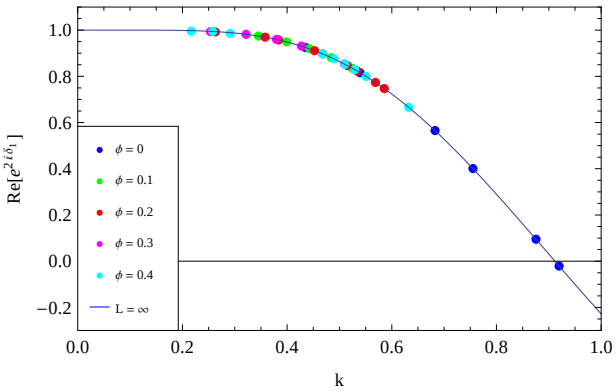

(b) twisted boundary conditions ($L = 20$)

Fig. 7: The reconstructed scattering phase shift $\delta_1(k)$ using the Lüscher formula with twisted boundary conditions. For futher information on this example see appendix B

shows the advantages of the twisted boundary conditions, since the number of points that could be reconstructed from one single volume could be improved. Also the distances between the individual points is much smaller, so that is would also be possible to calculate the derivative of the scattering phase shift, which is needed for equation (7).

7 Conclusion

Given the highly accurate determinations of the R ratio in e^+e^- experiments, where now even the dominant isospin breaking effects are taken into account, it is a challenge for lattice QCD to have a phenomenological impact on the determination of the hadronic vacuum polarization. In view of the upcoming $(g-2)_\mu$ experiment at Fermilab [30], an accuracy of well below 1% is called for on a_μ^{HLO}. We have outlined two alternatives to the direct calculation of the vacuum polarization. One option is the direct determination of the spectral function $\rho(s)$ in the threshold region along the lines of [10]. We described the determination of the scattering phases in the vector channel using twisted boundary conditions in section (6). A second promising approach is the calculation of the vector correlator $G(t)$

(defined in Eq. 72) in the region 0.5fm to 1.5fm or so, which provides a check on the R ratio in the energy region that makes the largest contribution to $a_\mu^{\rm HLO}$. We also considered the option of integrating $G(t)$ from t_0 to t_1, with the short-distance contribution treated in perturbation theory and the long-distance contribution obtained from the pion timelike form factor via the spectral representation, but it appears that the spectral function would have to be determined up to higher energies than the four-pion threshold for this strategy to be practical.

As a new idea we proposed to turn the table around and exploit the accurate knowledge of the vector spectral function to define a reference scale τ_0 in QCD which can be determined accurately and reliably. We believe that the only real difficulty could arise from finite-size effects, which should therefore be investigated numerically and analytically.

We have made first steps to study the finite-size effects affecting the calculation of the vacuum polarization and the hadronic contribution to $(g-2)_\mu$. In section (3), we have analyzed the tensor structure of the polarization tensor on the torus, and find that for generic values of the momentum, two functions invariant under the transformations of the cubic group $H(3)$ characterize the vector current correlator. This allows one to perform various tests for finite-size effects. Based on current conservation, we also derived a sum rule for the difference of the infinite-volume spectral function and the finite-temperature/finite-volume spectral function, Eq. (69). Then focussing on the spatial current correlator projected onto zero spatial momentum, we analyzed the contributions of different states as a function of Euclidean time. At large times, the relative finite volume effects become order unity, due to the discreteness of the two-pion states on the torus. This contribution however only represents a few percent of $a_\mu^{\rm HLO}$, due to the dominance of the ρ resonance in this quantity. We plan to study the finite-size effects of this contribution in the near future.

Acknowledgments

We thank Hartmut Wittig, Michele Della Morte, Benjamin Jäger and Andreas Jüttner for helpful discussions and for providing the lattice data displayed in Fig. (2). H.M. also thanks Achim Denig for helpful discussions.

A Finite-volume effects on the low-energy contribution to $a_\mu^{\rm HLO}$

In dealing with the different scales of the problem we will consider that

$$\frac{m_\pi}{m_\mu} = \mathrm{O}(1). \tag{115}$$

Because of this relation, the kernel $\tilde{K}(t)$ cannot be expanded, neither in a small-t expansion, nor in a large-t expansion.

In the chiral regime, the lowest-lying states contributing are two-pion states. Let us call the ground state energy E_0. Roughly at E_0+2m_π begin the states with a four-pion component in their wavefunction which is not exponentially small in the volume. Since it is not known how to relate the relative weight of these components to inelastic $\pi\pi$ scattering in infinite volume, we choose t_1 in such a way that the contribution of these states is suppressed,

$$2m_\pi t_1 \gg 1. \tag{116}$$

We assume that the box is large, in the sense that

$$m_\pi L \gtrsim \pi. \tag{117}$$

If we also choose t_1 such that

$$t_1 \gg \frac{L}{\pi}, \tag{118}$$

then only the ground state contributes to $G(t)$ for $t \geq t_1$. Since all factors in the integrand are slowly varying, except for the exponential e^{-Et}, the contribution to a_μ is approximately

$$a_\mu^{>}(L,t_1) \simeq 4\alpha^2 m_\mu t_1^3 \tilde{K}(t_1) |A_0(L)|^2 \frac{e^{-E_0 t_1}}{E_0}, \tag{119}$$

where $A_0 = L^{3/2}\langle \mathrm{vac}|j(\boldsymbol{x})|\psi_0\rangle$ is the matrix element of the vector current between the lowest-lying (two-pion) state in the box and the vacuum; it is related to the pion form factor through Eq. (7). In infinite volume, the situation is different, because there are states arbitrarily close to $2m_\pi$, and we must integrate over them. We define

$$a_\mu^{>}(t_1) = \lim_{L\to\infty} a_\mu^{>}(L,t_1). \tag{120}$$

Using the spectral representation of the correlator, one finds

$$a_\mu^{>}(t_1) = 4\alpha^2 m_\mu \int_0^\infty \mathrm{d}\omega\, \omega^2 \rho(\omega^2) \int_{t_1}^\infty \mathrm{d}t\, t^3\, \tilde{K}(t)\, e^{-\omega t} \tag{121}$$

$$\simeq 4\alpha^2 m_\mu \tilde{K}(t_1) t_1^3 \int_0^\infty \mathrm{d}\omega\, \omega \rho(\omega^2) e^{-\omega t_1}. \tag{122}$$

The large value of t_1 dictates that only the small ω region contributes, where the spectral density coincides with the timelike pion factor, see Eq. (6). One then finds

$$a_\mu^{>}(t_1) \simeq 4\alpha^2 m_\mu t_1^3 \tilde{K}(t_1) \frac{|F_\pi(2m_\pi)|^2}{48\pi^2} \frac{3\sqrt{\pi}}{2} \frac{e^{-2m_\pi t_1}}{m_\pi^{1/2} t_1^{5/2}}. \tag{123}$$

Comparing Eq. (119) and (123), we see that the expression obtained in finite volume is parametrically different, because $\exp(-E_0(L)t_1) \ll \exp(-2m_\pi t_1)$. The finite-volume effect is order unity for this long-distance contribution.

If the box is very large, $m_\pi L \gg \pi$, the contribution $\Delta a_\mu(L,t_1)$ for $t_1 \lesssim \frac{L}{\pi}$ (but still $2m_\pi t_1 \gg 1$) will be affected only by a small relative finite-volume effect. In this regime, the energy gaps between the two-pion states is much smaller than m_π, so that the sum over states is a

good approximation to the integral over momenta in infinite volume. This regime was investigated in [34]. However, this regime is hardly realistically achievable with present computing resources, because the condition $m_\pi L \gg \pi$ implies that L must be 10fm at the very least when m_π is set to its physical value.

B Illustration with a potential well

In section (6) the scattering phase shifts calculated for the quantum mechanical potential well were shown as an example. This appendix describes how these scattering phase shifts were calculated.

The potential well is of the form

$$V(|\boldsymbol{r}|) = -\alpha \cdot \Theta(R - |\boldsymbol{r}|), \tag{124}$$

where R is the range of the potential and α its strength. For a comparison to the scattering phase shifts calculated using the Lüscher formula the scattering phase shift in infinite volume is needed. To solution to the Schrödinger equation

$$\Big[-\frac{1}{2\mu}\Delta + V(|\boldsymbol{r}|)\Big]\Psi(\boldsymbol{r}) = \frac{k^2}{2\mu}\Psi(\boldsymbol{r}) \tag{125}$$

is best defined piecewise

$$\Psi(\boldsymbol{r}) = \sum_{l=0}^{\infty}\sum_{m=-l}^{l} Y_{lm}(\theta,\phi)\begin{cases}\alpha_l j_l(kr) + \beta_l n_l(kr) & r \geq R\\ j_l(\tilde{k}r) & r \leq R.\end{cases} \tag{126}$$

Requiring smoothness of the solution and its derivative at $r = R$ leads to a system of equations for the coefficiants $\alpha_l(k)$, $\beta_l(k)$. Once these are calculated the scattering phase shift can be calculated using the formula

$$\delta_l(k) = \arctan\left[\frac{\beta_l}{\alpha_l}\right]. \tag{127}$$

In order to calculate the scattering phase shifts using the formula derived in section (6) the first step now is to calculate the spectrum in the box. The general solution of the Helmholtz equation is used to define a solution piecewise inside the box,

$$\Psi(\boldsymbol{r})\Big|_{|\boldsymbol{r}|\geq R} = \sum_{l=0}^{\Lambda}\sum_{m=-l}^{l} v_{lm} G^{\phi}_{lm}(\boldsymbol{r};k^2), \tag{128}$$

$$\begin{aligned}\Psi(\boldsymbol{r})\Big|_{|\boldsymbol{r}|\leq R} &= \sum_{l=0}^{\Lambda}\sum_{m=-l}^{l} a_{lm} Y_{lm}(\theta,\phi) j_l(\tilde{k}r)\\ &\quad + \sum_{l=\Lambda+1}^{\infty}\sum_{m=-l}^{l} a_{lm} Y_{lm}(\theta,\phi) j_l(kr).\end{aligned} \tag{129}$$

The advantage of this ansatz is that the general solution of the Helmholtz equation that is used already satisfies the twisted boundary conditions

$$\Psi(\boldsymbol{r} + \boldsymbol{n}L) = e^{i\,\boldsymbol{n}\cdot\boldsymbol{\phi}}\Psi(\boldsymbol{r}), \quad \boldsymbol{n} \in \mathbb{Z}^3. \tag{130}$$

To simplify the calculation and to study the effects of higher scattering phase shifts the angular momentum cutoff Λ was introduced in the same way as in section (6). Before matching both pieces of the solution at the boundary $r = R$, the solution outside the range of the potential can be rewritten as

$$\Psi(\boldsymbol{r}) = \sum_{l=0}^{\Lambda}\sum_{m=-l}^{l} v_{lm} G^{\phi}_{lm}(\boldsymbol{r};k^2) \tag{131}$$

$$\begin{aligned}&= \sum_{l'=0}^{\infty}\sum_{m'=-l'}^{l'} Y_{l'm'}(\theta\phi)\Big\{\\ &\quad j_{l'}(kr)\sum_{l=0}^{\Lambda}\sum_{m=-l}^{l} v_{lm}\frac{(-)^l k^{l+1}}{4\pi}\mathcal{M}^{\phi}_{lm;l'm'}\\ &\quad + \Theta(\Lambda - l')v_{l'm'}\frac{(-)^{l'}k^{l'+1}}{4\pi}n_{l'}(kr)\Big\}.\end{aligned} \tag{132}$$

Since the $Y_{lm}(\theta,\phi)$ are normal to each other one gets a homogeneous system of equations when equating the two pieces of the solution at $r = R$. The important point to note is that the equations for $l > \Lambda$ do not influence the spectrum, they merely determine the $a_{l>\Lambda,m}$ in terms of the $v_{l\leq\Lambda,m}$. The latter coefficients are determined by the equations $l \leq \Lambda$. One has $\Lambda + 1$ homogeneous equations for as many variables. According to a well known theorem a non-trivial solution to a set of homogeneous equations only exists when the determinant of the corresponding matrix vanishes. This condition yields the allowed k-values. For $\Lambda = 2$ for instance, the determinant of the matrix of coefficients is of the block-diagonal form

$$\begin{vmatrix}\boldsymbol{\Lambda 0} & 0 & 0\\ 0 & \boldsymbol{\Lambda 1} & 0\\ 0 & 0 & \boldsymbol{\Lambda 2}\end{vmatrix} = \det[\boldsymbol{\Lambda 0}]\cdot\det[\boldsymbol{\Lambda 1}]\cdot\det[\boldsymbol{\Lambda 2}] = 0 \tag{133}$$

so that it seperates. Since we are interested in the scattering phase shift δ_1 we only need to consider the determinant $\det[\boldsymbol{\Lambda 1}]$. The system of equations that needs to be solved is

$$0 = v_{1-1}\frac{k^2}{4\pi}\big[j_1(kR)\mathcal{M}_{1-1;1-1} + n_1(kR)\big] + a_{1-1}j_1(\tilde{k}R) \tag{134}$$

$$0 = v_{10}\frac{k^2}{4\pi}\big[j_1(kR)\mathcal{M}_{10;10} + n_1(kR)\big] + a_{10}j_1(\tilde{k}R) \tag{135}$$

$$0 = v_{11}\frac{k^2}{4\pi}\big[j_1(kR)\mathcal{M}_{11;11} + n_1(kR)\big] + a_{11}j_1(\tilde{k}R). \tag{136}$$

In this example the roots of the determinant were found by plotting the determinant as a function of k using *Mathematica* and then using the function `FindRoot`. The calculated k values can then be inserted into the Lüscher formula for twisted boundary conditions derived in section (6) to calculate the scattering phase shifts. The parameters that were used to obtain the figures 7a, 7b were $\alpha = 2$, $R = 2$ and $\mu = 1$.

References

1. F. Jegerlehner, *Hadronic contributions to the photon vacuum polarization and their role in precision physics*, *J.Phys.G* **G29** (2003) 101–110, [hep-ph/0104304].
2. F. Jegerlehner and A. Nyffeler, *The Muon g-2*, *Phys.Rept.* **477** (2009) 1–110, [arXiv:0902.3360].
3. T. Blum, *Lattice calculation of the lowest order hadronic contribution to the muon anomalous magnetic moment*, *Phys.Rev.Lett.* **91** (2003) 052001, [hep-lat/0212018].
4. C. Aubin and T. Blum, *Calculating the hadronic vacuum polarization and leading hadronic contribution to the muon anomalous magnetic moment with improved staggered quarks*, *Phys.Rev.* **D75** (2007) 114502, [hep-lat/0608011].
5. X. Feng, K. Jansen, M. Petschlies, and D. B. Renner, *Two-flavor QCD correction to lepton magnetic moments at leading-order in the electromagnetic coupling*, arXiv:1103.4818.
6. M. Della Morte, B. Jager, A. Juttner, and H. Wittig, *The leading hadronic vacuum polarisation on the lattice*, arXiv:1011.5793.
7. **HPQCD Collaboration** Collaboration, I. Allison *et. al.*, *High-Precision Charm-Quark Mass from Current-Current Correlators in Lattice and Continuum QCD*, *Phys.Rev.* **D78** (2008) 054513, [arXiv:0805.2999].
8. B. Lautrup, A. Peterman, and E. de Rafael, *Recent developments in the comparison between theory and experiments in quantum electrodynamics*, *Phys.Rept.* **3** (1972) 193–260.
9. C. Kim and C. Sachrajda, $K \to (\pi\pi)_{I=2}$ *decays and twisted boundary conditions*, *Phys.Rev.* **D81** (2010) 114506, [arXiv:1003.3191].
10. H. B. Meyer, *Lattice QCD and the Timelike Pion Form Factor*, arXiv:1105.1892.
11. M. Luscher, *Signatures of unstable particles in finite volume*, *Nucl. Phys.* **B364** (1991) 237–254.
12. X. Feng, K. Jansen, and D. B. Renner, *Resonance Parameters of the rho-Meson from Lattice QCD*, arXiv:1011.5288.
13. **CP-PACS Collaboration** Collaboration, S. Aoki *et. al.*, *Lattice QCD Calculation of the rho Meson Decay Width*, *Phys.Rev.* **D76** (2007) 094506, [arXiv:0708.3705].
14. M. Luscher, *Two particle states on a torus and their relation to the scattering matrix*, *Nucl.Phys.* **B354** (1991) 531–578.
15. **Particle Data Group** Collaboration, C. Amsler *et. al.*, *Review of particle physics*, *Phys. Lett.* **B667** (2008) 1.
16. B. B. Brandt, S. Capitani, D. Djukanovic, G. von Hippel, B. Jager, *et. al.*, *Wilson fermions at fine lattice spacings: scale setting, pion form factors and* $(g-2)_\mu$, *PoS* **LATTICE2010** (2010) 164, [arXiv:1010.2390].
17. F. Jegerlehner, *Muon g - 2 update*, *Nucl.Phys.Proc.Suppl.* **181-182** (2008) 26–31.
18. M. Davier, A. Hoecker, B. Malaescu, and Z. Zhang, *Reevaluation of the Hadronic Contributions to the Muon g-2 and to alpha(MZ)*, *Eur.Phys.J.* **C71** (2011) 1515, [arXiv:1010.4180].
19. K. Hagiwara, R. Liao, A. Martin, D. Nomura, and T. Teubner, $(g-2)_\mu$ *and* $\alpha(M_Z^2)$ *re-evaluated using new precise data*, arXiv:1105.3149.
20. M. Davier, S. Eidelman, A. Hocker, and Z. Zhang, *Confronting spectral functions from e+ e- annihilation and tau decays: Consequences for the muon magnetic moment*, *Eur.Phys.J.* **C27** (2003) 497–521, [hep-ph/0208177].
21. G. Amelino-Camelia, F. Archilli, D. Babusci, D. Badoni, G. Bencivenni, *et. al.*, *Physics with the KLOE-2 experiment at the upgraded DAϕNE*, *Eur.Phys.J.* **C68** (2010) 619–681, [arXiv:1003.3868].
22. **KLOE Collaboration** Collaboration, S. E. Muller *et. al.*, *Measurement of the pion form factor for* $M^2_{\pi\pi}$ *between 0.1 and 0.85* GeV^2 *with the KLOE detector*, *Chin.Phys.* **C34** (2010) 686–691, [arXiv:0912.2205].
23. **KLOE Collaboration** Collaboration, F. Ambrosino *et. al.*, *Measurement of* $\sigma(e^+e^- \to \pi^+\pi^-)$ *from threshold to 0.85* GeV^2 *using Initial State Radiation with the KLOE detector*, *Phys.Lett.* **B700** (2011) 102–110, [arXiv:1006.5313].
24. **BABAR Collaboration** Collaboration, B. Aubert *et. al.*, *Precise measurement of the* $e^+e^- \to \pi^+\pi^-(\gamma)$ *cross section with the Initial State Radiation method at BABAR*, *Phys.Rev.Lett.* **103** (2009) 231801, [arXiv:0908.3589].
25. M. Passera, W. Marciano, and A. Sirlin, *The Muon g-2 and the bounds on the Higgs boson mass*, *Phys.Rev.* **D78** (2008) 013009, [arXiv:0804.1142].
26. M. Della Morte and A. Juttner, *Quark disconnected diagrams in chiral perturbation theory*, *JHEP* **1011** (2010) 154, [arXiv:1009.3783].
27. M. Goeckeler *et. al.*, *Lattice Operators for Moments of the Structure Functions and their Transformation under the Hypercubic Group*, *Phys. Rev.* **D54** (1996) 5705–5714, [hep-lat/9602029].
28. H. B. Meyer, *Transport Properties of the Quark-Gluon Plasma – A Lattice QCD Perspective*, arXiv:1104.3708.
29. R. Baier, *R-charge thermodynamical spectral sum rule in N=4 Yang-Mills theory*, arXiv:0910.3862.
30. **E-989** Collaboration *http://gm2.fnal.gov/*.
31. T. Schaefer, *Euclidean Correlation Functions in a Holographic Model of QCD*, *Phys. Rev.* **D77** (2008) 126010, [arXiv:0711.0236].
32. R. Sommer, *A New way to set the energy scale in lattice gauge theories and its applications to the static force and alpha-s in SU(2) Yang-Mills theory*, *Nucl. Phys.* **B411** (1994) 839–854, [hep-lat/9310022].
33. K. Rummukainen and S. A. Gottlieb, *Resonance scattering phase shifts on a nonrest frame lattice*, *Nucl.Phys.* **B450** (1995) 397–436, [hep-lat/9503028].
34. C. Lin, G. Martinelli, C. T. Sachrajda, and M. Testa, *K* $\to$ *pi pi decays in a finite volume*, *Nucl.Phys.* **B619** (2001) 467–498, [hep-lat/0104006].